

https://doi.org/10.1070/QEL17964

Age-related changes in the viscoelasticity of rabbit lens characterised by surface wave dispersion analysis

H. Zhang, M. Singh, F. Zvietcovich, K. Larin, S. Aglyamov

Abstract. **The viscoelastic properties of the young and mature rabbit lenses *in situ* are evaluated using wave-based optical coherence elastography (OCE). Surface waves in the crystalline lens are generated using acoustic radiation force (ARF) focused inside the eyeball. Surface-wave dispersion is measured with a phase-stabilised optical coherence tomography (OCT) system. The Young's modulus and shear viscosity coefficient are quantified based on a Scholte wave model. The results show that both elasticity and viscosity are significantly different between the young and mature lenses. The Young's modulus of the lenses increased with age from 7.74± 1.56 kPa (young) to 15.15 ± 4.52 kPa (mature), and the shear viscosity coefficient increased from 0.55 ± 0.04 Pa s (young) and 0.86 ± 0.13 Pa s (mature). It is shown that the combination of ARF excitation, OCE imaging, and dispersion analysis enables nondestructive quantification of lenticular viscoelasticity *in situ* and shows promise for *in vivo* applications.**

Keywords: *crystalline lens, optical coherence elastography (OCE), viscoelasticity, acoustic radiation force (ARF).*

1. Introduction

The crystalline lens is an important element of the human eye because it is responsible for eye accommodation [1]. During aging, the lenticular biomechanical properties play critical roles in the development of presbyopia, which results in the age-related loss of accommodation [2–4]. Previous studies have shown that aging leads to an increase in lens stiffness in many species, including humans [5–13]. This increase in stiffness means that the lens is less responsive to mechanical stretching forces during accommodation, which decreases the ability of the lens to change its shape during accommodation [3, 14]. Despite the significant role of lenticular biomechanical properties in vision, there is a lack of currently available technologies that can safely and noninvasively measure the lens biomechanical properties inside the globe. While the changes in lens elasticity have been investigated in detail [5–11], only a few studies have measured changes in the lens viscous properties with age [7, 15, 16]. Complete information about the lens biomechanical properties, e.g., viscoelasticity, would enable a better understanding of accommodation and development of new approaches to restore accommodation [4, 17].

Elastography was formalised in the early 1990s as a technique for imaging the elastic properties of tissues [18]. Ultrasound elastography [18, 19] and magnetic resonance elastography [20] are two clinical elastography techniques that are capable of detecting diseases earlier than other methods. Although they have been used to assess lenticular biomechanical properties [10, 21–23], they have notable drawbacks in this particular use case, such as contrast, resolution, and motion sensitivity. Recently, Brillouin spectroscopy has also been utilised to measure the biomechanical properties of the lens noninvasively [6, 24, 25]. However, the link between the Brillouin shift and viscoelasticity is still unclear [26].

Optical coherence tomography (OCT) [27] based elastography, termed optical coherence elastography (OCE) [28], overcomes many of these drawbacks. OCE can measure lenticular biomechanical properties from the analysis of nanometre-scale displacements [29–31] that require minimal force, ensuring tissue integrity. In our previous work, we demonstrated that the biomechanical properties of the lens could be measured *in situ* and quantified lenticular biomechanical properties as a function of age and intraocular pressure using dynamic OCE [32–34]. Recently, we used wave-based OCE to show the correlation between lens opacity and elasticity during cold cataract formation and oxidative cataract formation in an *ex vivo* porcine model [35, 36]. However, these wave-based measurements relied on the wave group velocity, which is heavily influence by the frequency of the wave and can only provide estimates of elasticity.

On the other hand, spectral analysis of surface wave propagation can enable robust assessments of tissue viscoelasticity [37, 38], which could enhance biomechanical measurements of the lens. In this study, the viscoelasticity of rabbit crystalline lenses *in situ* was assessed by inducing mechanical waves with focused acoustic radiation force (ARF), which were then detected by a phase-stabilised OCE system. Dispersion analysis was combined with a Scholte wave propagation model to quantify the viscoelasticity of the crystalline lenses.

2. Materials and methods

2.1. Experimental setup

To measure the rabbit lenticular biomechanical properties, we utilised a phase-stabilised swept-source ARF–OCE sys-

H. Zhang, M. Singh, F. Zvietcovich Department of Biomedical Engineering, University of Houston, 3517 Cullen Blvd., Room 2027, Houston, TX 77204, USA;
K. Larin Molecular Physiology and Biophysics, Baylor College of Medicine, One Baylor Plaza, BCM335, Houston, TX 77030, USA; e-mail: klarin@central.uh.edu;
S. Aglyamov Department of Mechanical Engineering, University of Houston, 4726 Calhoun Rd., Room N207, Houston, TX 77204, USA; e-mail: saglyamo@central.uh.edu

Received 21 September 2021
Kvantovaya Elektronika **52** (1) 42–47 (2022)
Submitted in English

tem, which combines OCT with a co-focused single-element ultrasound transducer. Figure 1a shows the schematic of the experimental setup. The OCE system was based on a swept source laser (SL131090, Thorlabs Inc., Newton, NJ) with a centry wavelength of ~1300 nm, a bandwidth of ~100 nm, and sweep rate of 100 kHz. The axial resolution of the OCT system was approximately 8 μm. The full width at half maximum (FWHM) of the transverse Gaussian profile of the OCT beam at the imaging focal plane was approximately 14 μm. The displacement stability of the system was measured as 1.9 nm. The raw interference signal was resampled into the linear k domain followed by a fast Fourier transform. The phase data was extracted from the angle of the complex OCT data after Fourier transform. The phase data was then converted to real distance with a refractive index of the lens as 1.38 [39]. The received signal was directly transformed by inverse Fourier transform on the interference fringes with linear k-space [40–41]. The ARF transducer (ISO 304HP; CTS Valpey Corporation, Hopkinton, MA) had a diameter of approximately 15 mm and a focal length of about 19 mm operating at 3.5 MHz centre frequency. A 3.5 MHz sinusoidal wave was generated by a function generator (DG4062; Rigol Technologies, Beijing, China) and was gated to produce five single-tone bursts from 500 Hz to 2500 Hz with a 100 Hz increment. The signal for the transducer was amplified using a power amplifier (350L; Electronics & Innovation Ltd., Rochester, NY, USA). The ARF remotely perturbed the anterior apical surface of the crystalline lens through the cornea and the aqueous humour of the eyeball. A 3D printed cone was filled with ultrasound gel to couple the ARF from the transducer to the eye. Since the intraocular pressure (IOP) can have a noticeable effect on the lens stiffness, it was controlled at 10 mmHg with a closed-loop control system [42].

The transducer induced a low amplitude localised displacement (< 10 μm) at the apical surface of the lens inside the eyeball (Fig. 2), which then propagated as an elastic wave. The OCE system acquired successive M-mode images (n = 250) over a ~8.1 mm line, where the centre of the scan was at the apex of the lens [43]. The scan time for one position was approximately 48 ms, and the entire M–B-mode scan time was about 12 s. The temporal phase profiles were unwrapped,

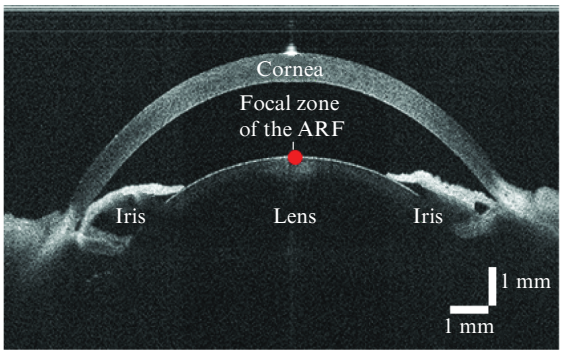

Figure 2. OCT image of the lens *in situ*.

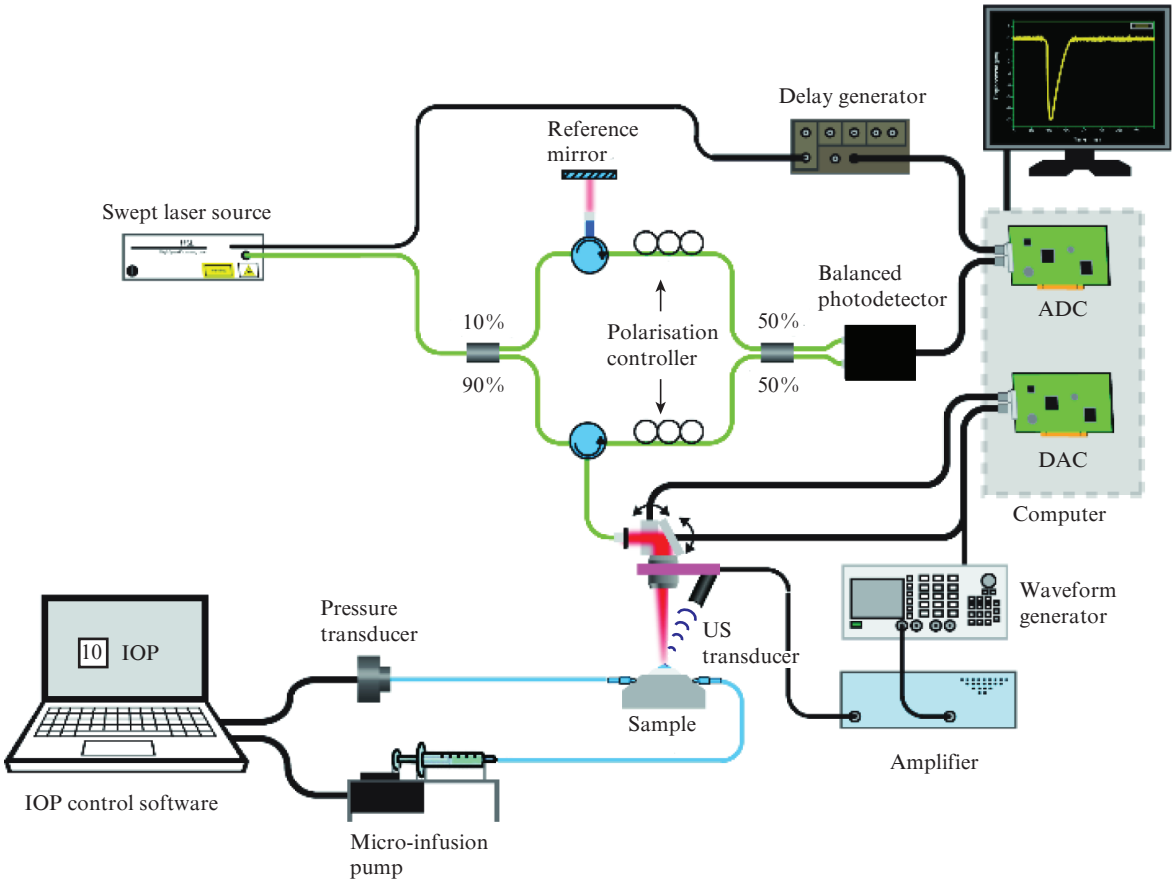

Figure 1. (Colour online) Schematic of the ARF-OCE system for *in situ* lens measurement.

converted to displacement, and corrected for surface compensation and refractive index mismatching artifacts [44]. The displacement profiles along the whole propagation path on the surface of the lens were then processed by a cross-correlation algorithm to obtain the elastic wave propagation delays [45] at each frequencies. The slope of a least-squares regression linear fit of the propagation delay to the propagation distance was the wave propagation speed. The fitting was performed from ~0.5 mm away from the excitation to remove the influence of near-field effects.

2.2. Sample preparation

Whole rabbit eyes (Pel-Freez Biologicals, LLC, Rogers, AR) were shipped overnight on ice. The eyes were separated into two groups: young (from 2 to 3-months old, $N = 5$) and mature (over 6-months old, $N = 10$). All experiments were performed immediately after receiving the eyes. The eye globes were kept in a 1X PBS solution at room temperature to keep the globe hydrated. The samples were placed in a 3D-printed eye holder during the experiments to eliminate bulk motion and for IOP control as mentioned earlier. After the experiments, all lenses were enucleated to measure the size and mass.

2.3. Wave propagation model

To evaluate age-related changes in the viscoelastic properties of the rabbit lenses quantitatively, we used a Kelvin–Voigt viscoelastic model of the tissue and Scholte wave model [46, 47], which matched the boundary conditions of the lens in the eye-globe (fluid on the anterior surface). We assumed that the lens thickness was significantly greater than mechanical wave wavelength in our frequency range (500–2500 Hz). The phase velocity of Scholte wave with a Kelvin–Voigt viscoelastic model of the tissue can be represented as:

$$c_S(\omega) = 0.84\sqrt{\frac{2(\mu_1^2 + \omega^2\mu_2^2)}{\rho(\mu_1 + \sqrt{\mu_1^2 + \omega^2\mu_2^2})}}, \quad (1)$$

where c_S is the measured phase velocity, ω is the angular frequency, $\rho = 1.183$ kg m^{-3} is the lens density [48], μ_1 is the shear modulus, and μ_2 is the shear viscosity. After the measurements, Matlab (Mathworks, Natick, MA) curve fitting tool was used to fit the OCE measurements to the analytical model of wave propagation and estimate the Young's modulus, E, based on the assumption of incompressibility ($E = 3\mu_1$) [49].

3. Results

Table 1 shows the lens parameters of young and mature rabbits.

Table 1. Size and mass of the rabbits' lenses.

Lens parameters	Young rabbits (2–3 months), $N = 5$	Mature rabbits (> 6 months), $N = 10$
Diameter/mm	5.98 ± 0.42	7.99 ± 0.52
Height/mm	9.29 ± 0.45	11.12 ± 0.42
Mass/g	0.33 ± 0.07	0.70 ± 0.07

Figure 3 shows the dispersion of the elastic wave (i.e., phase velocities) for representative lenses from (a) young rabbit group and (b) mature group and their respective fitting curves obtained using Eqn 1. The phase velocity of the young lens changed from ~1.4 m s^{-1} at 500 Hz to ~2.9 m s^{-1} at 2500 Hz. The phase velocity of the mature lens changed from ~1.8 m s^{-1} at 500 Hz to ~3.4 m s^{-1} at 2500 Hz. Based on the curve fitting, the Young's modulus of the young lens was estimated as 6.6 kPa (95% confidence bounds [5.1, 7.8] kPa) and the shear viscosity was 0.54 Pa s (95% confidence bounds [0.53, 0.56] Pa·s). The R^2 value of the fitting was 0.99. The Young's modulus of the mature lens was 15.6 kPa (95% confidence bounds [13.2, 17.7] kPa) and the shear viscosity was 0.83 Pa s (95% confidence bounds [0.80, 0.85] Pa s). The R^2 value of the fitting was 0.97.

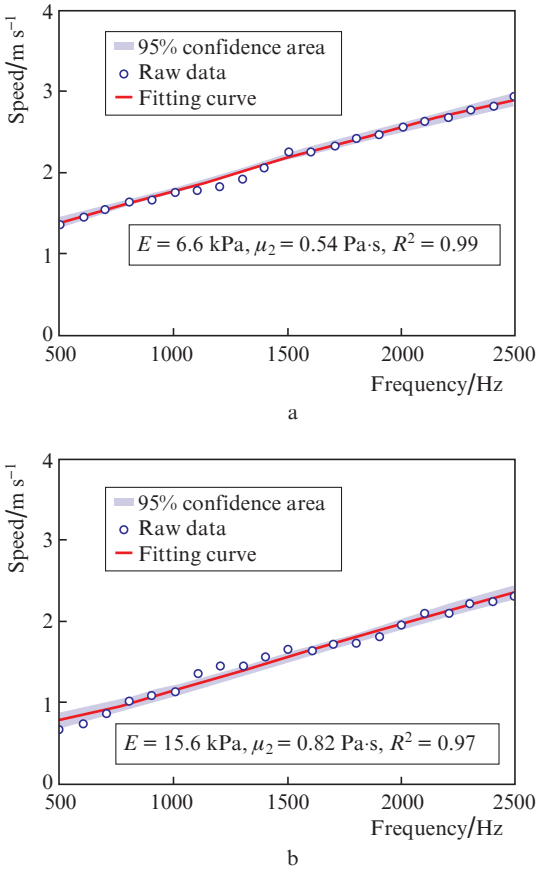

Figure 3. (Colour online) (blue circles) OCE-measured dispersion curves for the elastic wave propagation at the lens surface and (red line) fitting by the Scholte wave model for (a) one young lens and (b) one mature lens. The blue shaded region is the 95% confidence interval of the fit, and the viscoelastic parameters and fitting are labelled on each plot.

With the Young's modulus and the shear viscosity coefficient calculated by the curve fitting method, the average wave dispersion of each group of lenses was calculated. Figure 4 shows the average elastic wave dispersion curves for all lenses of each age group and their respective fitting to the mechanical model. It is obvious that the mature lenses had greater phase velocities in full frequency range than the young lens, indicating a greater stiffness.

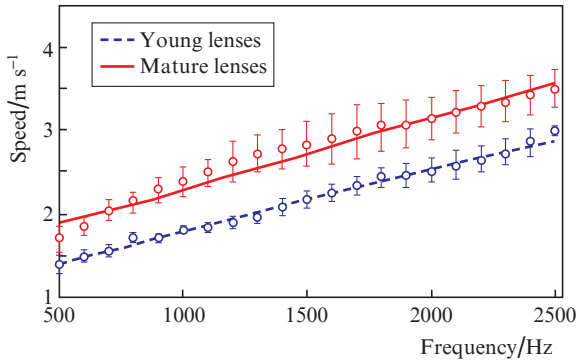

Figure 4. (Colour online) Average elastic wave dispersion curves of the young ($N = 5$) and mature ($N = 10$) lenses and the fit to the mechanical model using Eqn 1. The error bars show the intra-group standard deviation for each frequency.

The summary of the Young's modulus and the shear viscosity estimations is shown in Fig. 5. The results clearly show that the mature lenses are stiffer and more viscous than the young lenses, confirming our previous results with bovine and rabbit lenses (15, 16). Student's *t*-test was used to check the statistical significance of the difference between the two age groups. The average Young's modulus of the young lenses (7.74 ± 1.56 kPa) was significantly lower than average Young's modulus of the mature lenses (15.15 ± 4.52 kPa) ($P < 0.001$). The shear viscosity coefficient of the young lenses (0.55 ± 0.04 Pa s) was also significantly lower than that of the matured lenses (0.86 ± 0.13 Pa s) ($P = 0.013$). The trend is in agreement with our previous results in rabbit lenses based on the localised damping [15].

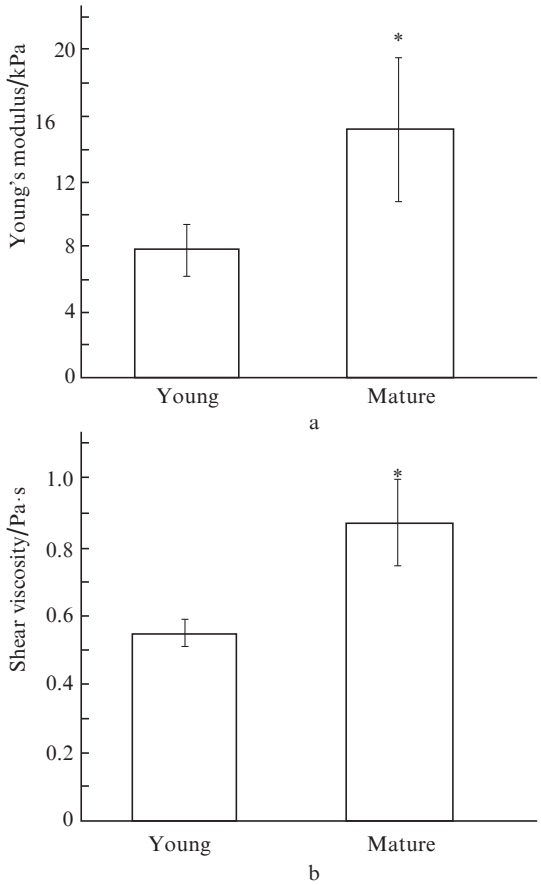

Figure 5. (a) Young's modulus and (b) shear viscosity coefficient of the young and matured lenses estimated based on the viscoelastic model. The asterisks indicate statistical significance ($P < 0.05$) determined by Student's *t*-test.

4. Discussion

In this work, we utilised ARF to induce elastic waves at different frequencies in young and mature rabbit lenses *in situ* at a controlled IOP. The mechanical waves were detected by the OCE system, and the wave dispersion was used in an analytical model to quantify the viscoelasticity of the lenses. The results show that the mature lenses were stiffer and more viscous than the young lenses.

This tendency is in agreement with the results of our previous work, where the viscoelastic properties of the rabbit lenses were evaluated based on the measurement of the localised displacement temporal dynamics at the point of ARF excitation [15]. However, both the values of Young's modulus and shear viscosity coefficient obtained in this work are greater than in our previous results, where the Young's modulus and shear viscosity coefficient were 2.5 kPa and 0.37 Pa s, respectively, for the young lenses, and 7.4 kPa and 0.57 Pa s for the mature lenses [15]. Still, in both studies the increase in stiffness with age is more pronounced than the increase in viscous coefficient. The difference in the estimated values could be explained by the difference in the measurement methods and the boundary conditions of the models. Previously, we used free boundary conditions on the lens surface [15], while in this study a more appropriate liquid–solid interaction was used.

One of the limitations of this surface wave-based technique is the limited ability to quantify the spatial distribution of the viscoelastic properties in the lens, particularly the stiffness gradient along the lens optical axis [8]. To overcome this limitation, we have recently demonstrated a multimodal optical elastography technique based on OCE and Brillouin spectroscopy [27]. This method overcomes the depth limitations of OCE due to the limited optical scattering in the lens and the semi-quantitative nature of Brillouin spectroscopy.

Our measurements were performed using the combined ARF-OCE system, and there are several different methods that can be applied to measure lenticular viscoelasticity, such as ultrasound elastography, uniaxial mechanical testing, and rheometry. Li et al. [12] applied ARF–OCE to measure the elasticity of rabbit lenses of different age groups *in vivo*. Their results show that the 8-week old rabbit lens had a Young's modulus of ~10 kPa [12]. Wang et al. [13] applied mechanical testing to measure the elasticity of the rabbit lens *ex vivo* and ultrasound elastography to measure the elasticity of the rabbit lens *in vivo*. Mechanical testing results showed that the Young's modulus of 7-month old rabbit lenses was 16.16 ± 1.85 kPa, and the ultrasound elastography measured the average Young's modulus of 2-month rabbit lens as ~6.75 kPa and that of 7-month rabbit lens was 15.87 kPa [13]. Zhang et al. [10] also applied ultrasound elastography to measure the elasticity of the rabbit lens *in vivo*. Their results show that the average Young's modulus of the 2-month old rabbit lens was about 5.7 kPa, and that of the 5-month old rabbit lens was about 15.87 kPa [10]. All these studies demonstrate that the Young's modulus of the rabbit lens increases during the aging process and had relatively similar results in age-matched samples where applicable.

Current studies of the lens viscosity are scarce and use different experimental and analytical approaches. Elrefaei et al. [50] vibrated the rabbit lens in different ultrasound environments to measure lenticular viscosity. Their results shows that the viscosity coefficient of the rabbit lens did not exceed 0.3 Pa s, but the authors did not note the age of the samples. Schachar et al. [51] used a shear rheometer on porcine lenses and estimated the viscosity coefficient as 0.16 ± 0.1 Pa s. The same approach was used to determine the viscoelastic properties of fresh human lenses under 40 years of age [7], where the dynamic viscosity at 75 Hz was 0.33 Pa s and 0.35 Pa s for nucleus and cortex, respectively, but no significant age dependence was observed. Yoon et al. compared the viscoelastic properties of the young (6 month old) and mature (25–30 month old) bovine lenses based on the measurement of laser-induced microbubbles in the lens [16]. The shear viscosity coefficient of the mature lenses (1.32 ± 0.12 Pa s) was greater than the young lenses (1.06 ± 0.12 Pa s) [16]. Overall, comparison of literature data is limited by the small number of studies and a range of experimental methods, but the results do show relatively similar shear viscosity coefficients.

In addition to material properties, the geometry of the lens can affect mechanical property measurements. For example, Sorsby et al. [52] found the radius of curvature of front surface of rabbit lens increased from 5.2 ± 0.42 mm at 7-weeks age to 6.1 ± 0.37 mm at 20-weeks age. However, the arc length difference between the lenses of two ages was about 7.5%, which is much smaller than the difference between the phase velocities of the young and mature lenses for the same frequencies shown in Fig. 4. Our previous results of FEM simulations and experimental studies for corneal like structures demonstrated that the elastic wave speed is inversely proportional to the radius of curvature [53]. Therefore, the increase in the lens curvature with age unlikely results in the increase of the phase velocity. The axial length also changes with age as Table 1 shows, while the wave model utilised in this work assumes a semi-infinite medium. At the worst-case scenario, i.e., the lowest frequency (500 Hz) and highest wave speed at this frequency (2 m s^{-1}), the mechanical wave wavelength is ∼4.0 mm. Hence, the assumption of a semi-infinite medium is reasonably sound given that the mechanical wave wavelength is less than the thickness. Therefore, we assume that the changes in the geometry of the lens during the growth i.e. the curvature and axial length may not be considered as a key factor affecting the phase velocities of the lens. This assumption, however, should be verified in future studies.

5. Conclusions

Thus, we applied, for the first time to our knowledge, OCE to measure the dispersion of the surface waves in rabbit crystalline lenses *in situ*. The elastic and viscous moduli of the lenses were significantly greater in the mature lenses as compared to the young lenses. The results show that the combination of ARF and OCE can be effectively used to quantify the age-related changes in lens viscoelasticity noninvasively. Our future work is focused on *in vivo* measurements and the development of more robust mechanical wave models.

Acknowledgements. This research was funded by the National Institutes of Health (Grant Nos R01EY022362 and R01EY030063).

References

1. Chien C.H., Huang T., Schachar R.A. *J. Biomech*., **39** (4), 672 (2006).
2. Koretz J.F., Cook C.A., Kaufman P.L. *Invest. Ophthalmol. Vis. Sci*., **38** (3), 569 (1997).
3. Lanchares E., Navarro R., Calvo B. *J. Optometry*, **5** (3), 110 (2012).
4. Glasser A. *Clin. Exp. Optometry*, **91** (3), 279 (2008).
5. Erpelding T.N., Hollman K.W., O'Donnell M. *Exp. Eye Res*., **84** (2), 332 (2007).
6. Scarcelli G., Kim P., Yun S.H. *Biophys. J*., **101** (6), 1539 (2011).
7. Schachar R.A., Chan R.W., Fu M. *Br. J. Ophthalmol*., **95**, 1010 (2011).
8. Weeber H.A., Eckert G., Pechhold W., van der Heijde R.G. *Graefes Arch. Clin. Exp. Ophthalmol.*, **245** (9), 1357 (2007).
9. Weeber H.A., Eckert G., Soergel F., Meyer C.H., Pechhold W., van der Heijde R.G. *Exp. Eye Res*., **80** (3), 425 (2005).
10. Zhang X.Y., Wang Q.M., Lyu Z., Gao X.H., Zhang P.P., Lin H.M., Guo Y.R., Wang T.F., Chen S.P., Chen X. *Biomed. Eng. Online*, **17** (1), 75 (2018).
11. Hollman K.W., O'Donnell M., Erpelding T.N. *Exp. Eye Res*., **85** (6), 890 (2007).
12. Li Y., Zhu J., Chen J.J., Yu J.X., Jin Z., Miao Y.S., et al. *Apl. Photonics*., **4** (10), 106104 (2019).
13. Wang Q.M., Zhu Y., Shao M., Lin H.M., Chen S.P., Chen X., et al. *Exp. Eye Res*., **184**, 258 (2019).
14. Xiang Y., Fu T., Xu Q.F., Chen W., Chen Z.Q., Guo J.M., et al. *Sci. Rep-Uk*, **11** (1), 6688 (2021).
15. Wu C., Han Z., Wang S., Li J., Singh M., Liu C-h., et al. *Invest. Ophthalmol. Vis. Sci*., **56** (2), 1292 (2015).
16. Yoon S., Aglyamov S., Karpiouk A., Emelianov S. *Ultrasound Med. Biol*., **39** (6), 1120 (2013).
17. Reggiani Mello G.H., Krueger R.R. *Int. Ophthalmol. Clin*., **51** (2), 87 (2011).
18. Ophir J., Cespedes I., Ponnekanti H., Yazdi Y., Li X. *Ultrasonic Imaging*, **13** (2), 111 (1991).
19. Bercoff J., Tanter M., Fink M. *IEEE Transact. Ultrason. Ferroelect. Freq. Control*., **51** (4), 396 (2004).
20. Muthupillai R., Lomas D.J., Rossman P.J., Greenleaf J.F., Manduca A., Ehman R.L. *Science*, **269** (5232), 1854 (1995).
21. Detorakis E.T., Drakonaki E.E., Ginis H., Karyotakis N., Pallikaris I.G. *Acta. Med. (Hradec Kralove)*, **57** (1), 9 (2014).
22. Park S., Yoon H., Larin K.V., Emelianov S.Y., Aglyamov S.R. *Phys. Med. Biol*., **62** (3), N45 (2017).
23. Zhou H.Y., Yan H., Yan W.J., Wang X.C., Li Q.Y. *Int. J. Ophthalmol.-Chi*., **13** (3), 399 (2020).
24. Reiss S., Sperlich K., Hovakimyan M., Martius P., Guthoff R.F., Stolz H., Stachs O. *IEEE Transact. Biomed. Eng*., **59** (8), 2348 (2012).
25. Ambekar Y., Singh M., Zhang J.T., Nair A., Aglyamov S.R., Scarcelli G., Larin K.V. *Biomed. Opt. Express*, **11** (4), 2041 (2020).
26. Antonacci G., Pedrigi R.M., Kondiboyina A., Mehta V.V., de Silva R., Paterson C., Krams R., Török P. *J. R. Soc. Interface*., **12** (112), 20150843 (2015).
27. Huang D., Swanson E.A., Lin C.P., Schuman J.S., Stinson W.G., Chang W., et al. *Science*, **254** (5035), 1178 (1991).
28. Schmitt J. *Opt. Express*, **3** (6), 199 (1998).
29. Kennedy B.F., Wijesinghe P., Sampson D.D. *Nat. Photonics*, **11** (4), 215 (2017).
30. Kirby M.A., Pelivanov I., Song S., Ambrozinski L., Yoon S.J., Gao L., et al. *J. Biomed. Opt*., **22** (12), 1 (2017).
31. Larin K.V., Sampson D.D. *Biomed. Opt. Express*, **8** (2), 1172 (2017).

32. Wu C., Aglyamov S.R., Han Z.L., Singh M., Liu C.H., Larin K.V. *Biomed. Opt. Express*, **9** (12), 6455 (2018).
33. Wu C., Aglyamov S.R., Zhang H., Larin K.V. *Quantum Electron*., **49** (1), 20 (2019) [*Kvantovaya Elektron*., **49** (1), 20 (2019)].
34. Zhao L., Chen X.J., Zhu J., Xi Y.B., Yang X., Hu L.D., Ouyang H., Patel S.H., Jin X., Lin D., Wu F., Flagg K., Cai H., Li G., Cao G., Lin Y., Chen D., Wen C., Chung C., Wang Y., Qiu A., Yeh E., Wang W., Hu X., Grob S., Abagyan R., Su Zh., Tjondro H.C., Zhao X.-J., Luo H., Hou R., Jefferson J., Perry P., Gao W., Kozak I., Granet D., Li Y., Sun X., Wang J., Zhang L., Liu Y., Yan Y.-B., Zhang K. *Nature*, **523** (7562), 607 (2015).
35. Zhang H., Singh M., Nair A., Larin K.V., Aglyamov S.R. *Photonics*, **8** (6), 207 (2021).
36. Zhang H., Wu C., Singh M., Nair A., Aglyamov S., Larin K. *J. Biomed. Opt*., **24** (3), 1 (2019).
37. Han Z.L., Li J.S., Singh M., Wu C., Liu C.H., Wang S., et al. *Phys. Med. Biol*., **60** (9), 3531 (2015).
38. Han Z.L., Singh M., Aglyamov S.R., Liu C.H., Nair A., Raghunathan R., et al. *J. Biomed. Opt*., **21** (9), 090504 (2016).
39. Garner L.F., Smith G. *Optometry Vision Sci*., **74** (2), 114 (1997).
40. Choma M.A., Ellerbee A.K., Yang C.H., Creazzo T.L., Izatt J.A. *Opt. Lett*., **30** (10), 1162 (2005).
41. Manapuram R.K., Manne V.G.R., Larin K.V. *J. Appl. Phys*., **105** (10), 102040 (2009).
42. Twa M.D., Li J., Vantipalli S., Singh M., Aglyamov S., Emelianov S., et al. *Biomed. Opt. Express*, **5** (5), 1419 (2014).
43. Wang S., Larin K.V. *Opt. Lett*., **39** (1), 41 (2014).
44. Song S., Huang Z., Wang R.K. *J. Biomed. Opt*., **18** (12), 121505 (2013).
45. Wang S., Lopez A.L., 3rd, Morikawa Y., Tao G., Li J., Larina I.V., et al. *Biomed. Opt. Express*, **5** (7), 1980 (2014).
46. Zvietcovich F., Yao J.N., Rolland J.P., Parker K.J. *Proc. SPIE*., **9710,** 97100Z (2016).
47. Ewing W.M., Jardetzky W.S., Press F. *Elastic Waves in Layered Media* (Graw-Hill Book Company, Inc; 1957).
48. Vilupuru A.S., Glasser A. *Ophthalmol. Physiolog. Opt*., **21** (4), 296 (2001).
49. Aglyamov S.R., in *Tissue Elasticity Imaging. 1* (Elsevier, 2020) Chap. 2, pp 17–42.
50. Elrefaei F.M., Hassan M.S., Ibrahim I.H., Afify R.N. *J. Global Biosci*., **4** (8), 3229 (2015).
51. Schachar R.A., Chan R.W., Fu M. *Brit. J. Ophthalmol*., **91** (3), 366 (2007).
52. Sorsby A., Stone J., Leary G.A., Sheridan M. *Brit. J. Ophthalmol*., **44**, 467 (1960).
53. Han Z., Li J., Singh M., Aglyamov S.R., Wu C., Liu C-H., et al. *Appl. Phys. Lett*., **106**, 233702 (2015).